

1 **Chemical Structure of Medium-Scale Liquid Pool Fires**

2 Ryan Falkenstein-Smith*, Kunhyuk Sung, Jian Chen, and Anthony Hamins*

3 National Institute of Standards and Technology, 100 Bureau Dr., Gaithersburg, Maryland, USA
4 ryan.falkenstein-smith@nist.gov and anthony.hamins@nist.gov

5 *Corresponding authors

6 **Highlights:**

- 7 • Gas species and soot measurements of steadily burning methanol, ethanol, and acetone
8 30 cm pool fires are reported.
- 9 • Measurements were verified using theoretical gas species ratios.
- 10 • Flame structure was found to be in agreement with previous work.
- 11 • Gas species concentrations were shown to vary between different fuels.

12 **Abstract:** This work documents a series of time-averaged local gas species measurements made
13 throughout the centerline profile of 30 cm methanol, ethanol, and acetone pool fires steadily
14 burning in a quiescent environment. All gas species measurements were obtained using extractive
15 sampling, then analyzed using a gas chromatograph equipped with a mass spectrometer detector
16 (GC/MS). The volume fraction of each species was calculated via the number of moles identified
17 by the GC/MS at each location along the fire's centerline. Soot mass fractions were also measured
18 during the gas-sampling process. The gas species and soot mass fractions were compared at
19 different locations for fires burning three fuels.

20 **Keywords:**

21 Moderately-sized pool fires, acetone fuel, ethanol fuel, methanol fuel, gas species measurements

22 **1. Introduction**

23 Computational fire models, such as the Fire Dynamic Simulator (FDS) [1], have increased in
24 usage within the fire protection engineering community due to their effectiveness, ease of use, and
25 the decreased cost of computational power. To be reliable, fire models require validation to aid in
26 their development and confirm their accuracy and limitations. The objective of this research is to
27 provide experimental data for use in fire model development and evaluation.

28 Pool fires are a fundamental combustion configuration of interest. In a pool fire, the fuel surface is
29 flat and horizontal, which provides a simple and well-defined configuration for testing models and
30 furthering the understanding of fire phenomena. In moderate and large-scale pool fires, radiative
31 heat transfer is the dominant mechanism of heat feedback to the fuel surface. Species
32 concentrations and temperatures control the radiative heat transfer. An area of particular interest
33 is the fuel rich core just above the pool surface, where vaporizing fuel molecules and other gas

34 species can absorb energy that otherwise would have been transferred to the fuel surface. An
35 essential component in this zone is the spatial distribution of gas-phase chemical species. It is
36 well known that the local gas species within a fire is a critical component of its structure.
37 However, there are few studies in the pool fire literature that have reported local chemical species
38 measurements, which elucidate the chemical structure of the fire and provide insight on its
39 kinetic, heat, and mass transfer processes.

40 The purpose of this study is to characterize the spatial distribution of stable gas-phase chemical
41 species in moderate-scale liquid pool fires steadily burning in a well-ventilated, quiescent,
42 environment. Here, methanol, ethanol, and acetone are the fuels of interest. Contrary to ethanol
43 and acetone, fires established using methanol are unusual as no carbonaceous soot is present or
44 emitted.

45 In this study, all gas species measurements are made in a 30 cm diameter pool fire using liquid
46 fuels. These fuels are selected since the measurements complement results from previous studies,
47 including analyses of the mass burning rate, the temperature and velocity fields, radiative
48 emission, flame height, and pulsation frequency [2, 3, 4, 5]. Additional characterization of these
49 fires enables a more comprehensive understanding of its detailed structure, enhancing the
50 understanding of fire physics.

51 **2. Experimental Methods**

52 **2.1 Pool Burner Setup**

53 A circular, stainless-steel pan with an outer diameter of 30 cm, 15 cm deep, and a 0.16 cm wall
54 thickness was used as the pool burner. As shown in Fig. 1, the burner has an overflow basin,
55 which extended 3.0 cm beyond the burner wall. The burner is fitted with legs such that the burner
56 rim was 30 cm above the ground. The bottom of the burner was maintained at a constant
57 temperature by flowing water ($20\text{ }^{\circ}\text{C} \pm 3\text{ }^{\circ}\text{C}$) through the 3 cm section on the bottom of the fuel
58 pan. Additionally, a fuel level indicator was positioned near the center of the burner to monitor
59 the fuel level during burning.

60 The pool burner was located under a canopy hood surrounded by a 2.5 m x 2.5 m x 2.5 m
61 enclosure made of a double-mesh screen wall. The walls of the enclosure were formed by a
62 double layer wire-mesh screen (5 mesh/cm) to reduce the influence of ambient air flows that
63 could disrupt the flow field. All measurements were made once the mass burning rate reached
64 steady-state, achieved approximately 10 min after ignition.

65 The time-averaged mass burning rate, \dot{m} , was determined from the rate at which fuel was
66 delivered to the pool from a reservoir positioned on a mass load cell located outside the enclosure
67 and monitored by a data acquisition system (DAQ). The operator was able to observe a close up
68 of a slightly discernible dimple on the fuel surface using a live video feed. The fuel level was
69 maintained at 10 mm below the burner rim by manually adjusting the fuel flow with a needle
70 valve.

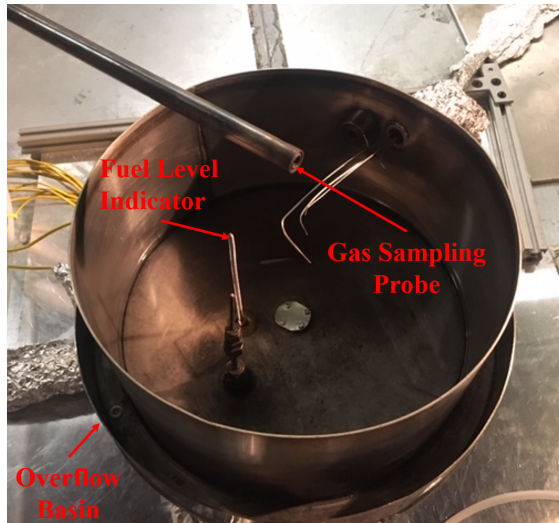


Fig. 1. 30 cm pool burner with fuel level indicator, overflow section, and water-cooled gas sampling probe.

71 The idealized heat release rate of each fuel, \dot{Q} , was calculated from Eq. 1 using the time-averaged
 72 mass loss measurements:

$$\dot{Q} = \dot{m} \Delta H_c \quad (1)$$

73 where ΔH_c is the heat of the combustion of the burned fuel provided by DIPPR[®] [7] and listed in
 74 Table 1.

75 The mean flame height was estimated from 3600 frames obtained from high-quality video
 76 recordings of the pool fire experiments, using a technique reported in Ref. [8]. Frames were
 77 processed using MATLAB's Image Processing Toolbox¹. Imported RGB images were
 78 decomposed into binary (black and white) images using a pre-set threshold level. The flame
 79 height for a single frame was defined as the distance between the pool surface and flame tip
 80 established using MATLAB software. All measurements were repeated, then averaged to provide
 81 mean values.

82 2.2 Temperature Measurements

83 Time-averaged temperature measurements were made along the pool fire centerline. The height
 84 locations ranged from 2 to 60 cm relative to the burner rim for all fires. Additional measurements
 85 were made higher, up to 100 cm, in the acetone fire to sample its taller flame. A fine S-type
 86 thermocouple with a diameter of 50 μm (P10R-001, OMEGA) was positioned onto a traverse

¹Certain commercial products are identified in this report to specify adequately the equipment used. Such identification does not imply a recommendation by the National Institute of Standards and Technology, nor does it imply that this equipment is the best available for the purpose.

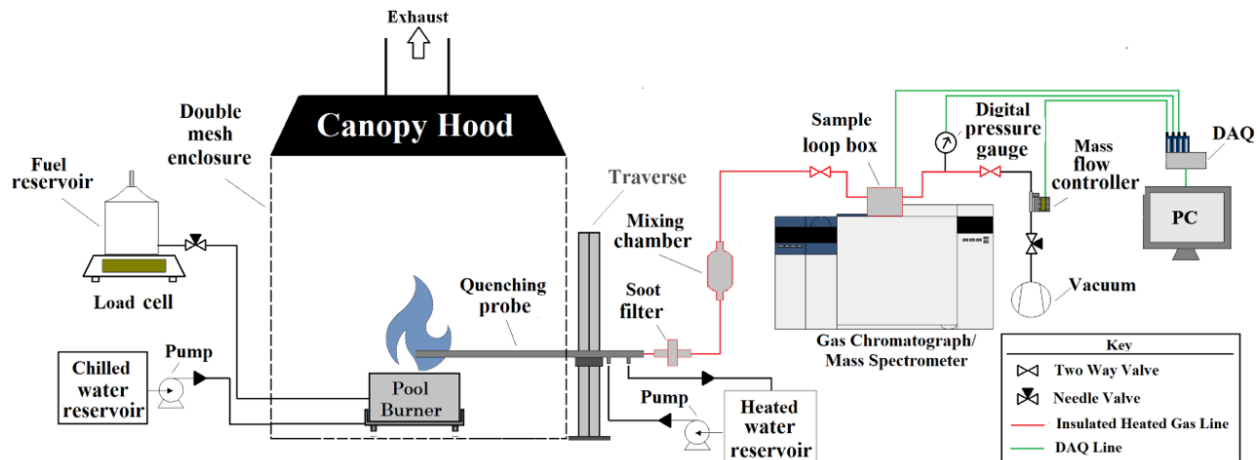


Fig. 2. A schematic of the extractive sampling setup used to extract and transport fire samples from the pool fire to the GC/MS.

87 such that the bare thermocouple bead was centered above the middle of the burner. The traverse
 88 controlled the position of the thermocouple relative to the burner rim as prompted via computer.
 89 Temperature measurements were sampled at 250 Hz for 2 min which represented more than 300
 90 fire pulsing cycles [9]. The thermal inertia and radiative heat loss associated with the
 91 thermocouple were corrected following Shaddix [10]. The temperature dependent emissivity of
 92 platinum was taken from Ref. [11]. The thermal inertia correction had little influence (< 5 K) on
 93 the mean temperature but significantly altered the RMS.

94 2.3 Measuring the Volume Fraction of Gas Species

95 Figure 2 displays the flow diagram for gas sampling into an Agilent 5977E Series Gas
 96 Chromatograph equipped with a mass spectrometer detector (GC/MS) fitted with a thermal
 97 conductivity detector (TCD). After achieving steady-state burning conditions, approximately
 98 10 min after ignition, flow was initiated by a vacuum pump located downstream from the GC/MS
 99 was initiated. Gas samples were collected using a water-cooled probe. The probe was composed
 100 of two concentric, stainless-steel tubes with outer annular coolant flow and inner, extracted,
 101 gas-sample flow. The inner and outer tube diameters were 8 mm and 16 mm, respectively. Water
 102 at 90 °C flowed through the sampling probe during the experiment. The remainder of the
 103 sampling line leading into the GC/MS was heated with electrical heating tape to 140 °C to prevent
 104 condensation of water and fuels in the line.

105 The gas sampling period varied from 12 to 25 min, depending on the sampling location within the
 106 fire. Ensuring that the gas sample had completely swept through the GC/MS sample loop, the
 107 sampling flow was controlled using a mass-flow controller (Alicat Scientific MC-Series) located
 108 in front of the vacuum pump within the sampling line. During the gas sampling procedure, the
 109 volumetric flow was approximately 0.2 SLPM, recorded using a DAQ at 2.0 Hz. The mass-flow
 110 controller also provided temperature readings of the gas flow.

111 After the gas sampling period, two quarter-turn valves located on opposite ends of the GC/MS
112 sample loop within the sampling line were closed. Once the sampled gas reached equilibrium,
113 pressure measurements, obtained from a digital pressure gauge (OMEGA DPG409-030DWU),
114 and temperature measurements, acquired by a K Type Thermocouple located at the GC/MS
115 sample loop injection port, were collected at 2.0 Hz for 50.0 s. After collecting pressure and
116 temperature measurements, the sampled gas was injected into the GC/MS.

117 The volume fraction, \bar{X}_i , was calculated from the ratio between the number of moles of a given
118 gas species, n_i , and the total number of moles, n_{tot} . The moles of a given species were identified
119 using the mass spectrometer and quantified from the TCD within the GC/MS. The total number of
120 moles was determined from the summation of moles for each species detected by the TCD.

$$\bar{X}_i = \frac{n_i}{n_{\text{tot}}} \quad (2)$$

121 The mass fraction, \bar{Y}_i , of each species i was calculated from the measured volume fraction, \bar{X}_i ,
122 using the following expression:

$$\bar{Y}_i = \frac{\bar{X}_i W_i}{W_{\text{tot}}} \quad (3)$$

123 where W_i is the molecular weight of a given species and W_{tot} is the average molecular weight of
124 the sample represented by

$$W_{\text{tot}} = \sum \bar{X}_i W_i \quad (4)$$

125 All measurements using the GC/MS were repeated at least twice along the centerline of the pool
126 fire, at the same positions as the temperature measurements. Gas species concentration
127 measurements made at the same location were averaged. The variance in the gas species volume
128 fraction was a function of position and species.

129 **2.4 Soot Mass Fraction Measurements**

130 Soot was collected simultaneously with gas samples using the sampling procedure described in
131 Section 2.3. Before a test, a desiccated 47.0 mm diameter polytetrafluoroethylene (PTFE) filter
132 was weighed and placed into an in-line stainless steel particulate filter holder. During an
133 experiment, the filter holder was positioned within the gas sampling line behind the sampling
134 probe and heated to 140 °C, using heating tape to prevent condensation of water and liquid fuels
135 on the filter. After testing, the PTFE filter was removed from the filter holder and dried in a
136 desiccator. After desiccating for 48 h, the PTFE filter's final weight was measured. Typically,
137 2 mg of soot was collected during the sampling period. To obtain a meaningful sample, the
138 sampling period varied from 12 min to 25 min depending on the sampling location within the fire.

139 After some tests, soot deposits were observed on the inner walls of the quenching probe.
140 Desiccated gun cleaning patches were used to collect soot on the inside of the sampling probe. At
141 least two patches were used to collect soot on the inside of the probe. Soot collection on the
142 inside of the probe concluded once a used patch was observed to have no soot. Patches were
143 weighed immediately before and 48 hrs after cleaning the inside of the probe. The soot collected

144 from the dry patches was accounted for when calculating the soot mass fraction. The portion of
145 the soot collected on the inner walls of the quenching probe relative to the PTFE filter varied
146 based on the sampling location. The mass of the PTFE filter and cleaning patches were measured
147 three times before and after each test.

148 The soot mass fraction, Y_s , was computed from the mass of the soot collected from the PTFE filter
149 and gun cleaning patches, m_s , the ratio of the mass-flow controller's temperature reading, T_∞ , to
150 the temperature at the probe entrance, T_g , the total mass of gas sampled, m_t , based on the
151 mass-flow controller readings:

$$Y_s = \frac{m_s T_\infty}{m_t T_g} \quad (5)$$

152 The total mass of gas sampled was estimated from the product of the average volumetric flow rate
153 measured by the mass-flow controller, \dot{V} , the density of the sample gas injected into the GC/MS,
154 ρ_g , and the gas sampling time, δt .

$$m_t = \dot{V} \rho_g \delta t \quad (6)$$

155 In Eq.6, the density of the sample gas was determined from the total mass detected in the TCD
156 chromatogram, m_{tot} , for the injected sample volume, V_s .

$$\rho_g = \frac{m_{tot}}{V_s} \quad (7)$$

157 **2.5 Uncertainty Analysis**

158 The expanded uncertainties of the mass burning rate, mean flame height, volume fraction of gas
159 species, and soot mass fractions were estimated through a combination of Type A and B
160 evaluation of standard uncertainty using a 95 % confidence interval and a coverage factor of 2.
161 The Type A evaluation of standard uncertainty was determined from the variance of repeated
162 measurements. The Type B evaluation of standard uncertainty was defined as the bias errors in the
163 instrumentation. The combined uncertainty of calculated parameters were estimated using the law
164 of propagation of uncertainty. The uncertainty of all measurements is discussed further in Ref. [6].

165 **3. Results**

166 **3.1 Flame Observations**

167 Figure 3 displays a series of snapshots depicting the puffing cycle for methanol, ethanol, and
168 acetone pool fires. A repeated cycle was observed in each of the pool fires; uniformly curved
169 flame sheets present at the burner rim repeatedly rolled towards the fire centerline to form a long
170 and narrow plume.

171 The shape and visible color of the fires differed between fuel types. The methanol fire appeared to
172 be completely blue, whereas the ethanol, and acetone fires were luminous and yellow. The
173 methanol pool fire was observed to exhibit a quasi laminar flame structure compared to the more
174 turbulent nature of fires seen for the other two fuels. The observed dynamic shapes were
175 consistent with previous experiments [3, 4, 5, 12, 13, 14].

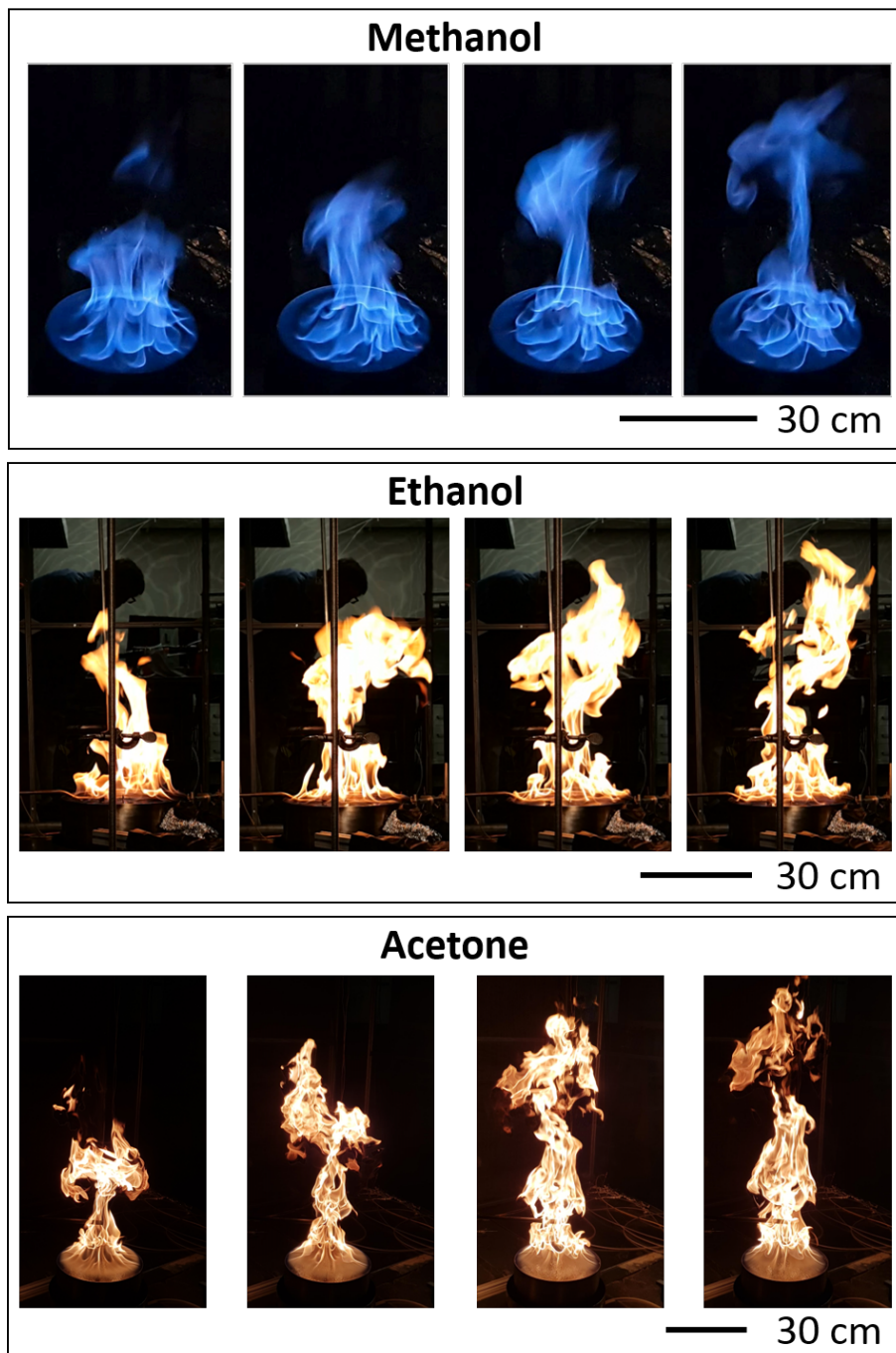


Fig. 3. Snapshots of the methanol (top), ethanol (middle), and acetone (bottom) pool fires during their pulsing cycles of frequency 2.6 Hz [9].

Table 1: List of measurements and thermochemical properties of fuels burning in a well-ventilated round 30 cm diameter pool fire burning in a quiescent environment. Measurement uncertainties are discussed in detail in Ref. [6].

Parameter (units)	Methanol	Ethanol	Acetone
Mass Burning Flux (g/m ² s)	12.4 ± 1.1	13.9 ± 0.8	17.6 ± 2.7
Heat Release Rate (kW)	17.4 ± 1.4	26.3 ± 1.5	35.5 ± 5.4
Mean Flame Height (cm)	36.4 ± 16.0	61.1 ± 28.2	91.5 ± 34.6
Heat of Combustion (kJ/g) [7]	19.9	26.8	28.6
C/H	3.0	4.0	6.0

176 The measured time-averaged burning flux and calculated ideal heat release rate are provided in
 177 Table 1. The heat release rate was calculated from Eq. 1. The time-averaged flame height reported
 178 in Table 1, of the methanol pool fire, was the shortest, followed by the ethanol, and then the
 179 acetone pool fires. In comparison to the measured mean flame height of each fuel, Heskestad's
 180 theoretical flame height, reported in Ref. [16], falls within the experimental uncertainty. The
 181 measurements in Table 1 are in agreement with measurements from Ref. [4] within experimental
 182 uncertainty.

183 3.2 Temperature and Gas Species Measurements of Methanol, Ethanol, and Acetone Pool 184 Fires

185 To account for the difference in height between the methanol, ethanol, and acetone pool fires, the
 186 mean flame height, H , of each fuel was converted to dimensionless distance, Z^* , which was
 187 calculated as follows:

$$z^* = H \left(\frac{\dot{Q}}{c_p \sqrt{g} \rho_o T_o} \right)^{\frac{2}{5}} \quad (8)$$

188 Here \dot{Q} is the heat release rate, g is the gravitational constant, and c_p and ρ_o are the specific heat
 189 and the density of air at room temperature, T_o .

190 Figure 4 shows the time-averaged corrected gas temperatures from the centerline of the methanol,
 191 ethanol, and acetone pool fires. The maximum mean temperature from each pool fire was found
 192 to peak at an approximate z^* of 0.6. Methanol was determined to have the highest mean
 193 temperature of 1316 K with ethanol and acetone exhibiting maximum mean temperatures of
 194 1281 K and 1190 K, respectively. The maximum mean temperature of fuels with higher heat
 195 release rates is shown to be lower compared to other fuels.

196 Figure 5 displays the volume fraction, \bar{X}_i , of major species centerline measurements as a function

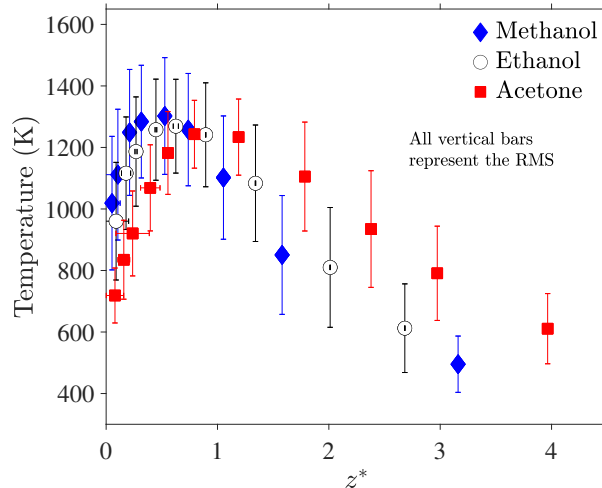


Fig. 4. Mean and RMS centerline temperature profiles of methanol, ethanol, and acetone pool fires during their pulsing cycles with z^* expanded uncertainty.

197 of Z^* along the centerline for the methanol, ethanol, and acetone fires. Major species detected in
 198 the TCD chromatogram include combustion reactants (fuels and oxygen, O_2), combustion
 199 products such as water, H_2O , and carbon dioxide, CO_2 , combustion intermediates such as carbon
 200 monoxide, CO , hydrogen, H_2 , and inert gases such as Nitrogen, N_2 , and Argon, Ar. Methane was
 201 detected and quantified in all fires. In the case of the ethanol and acetone fires, soot, benzene,
 202 acetylene, ethylene, and ethane were also detected and quantified. Trace amounts of other species
 203 were also detected including propene, acetaldehyde, and ethyl acetate, which is consistent with
 204 the literature [17, 18].

205 For all fuels, the fuel and oxygen volume fractions were largest and smallest, respectively, close
 206 to the fuel surface. The volume fraction of fuel did not reach 1.0, since the lowest position of gas
 207 species measurement for all fuels was 2 cm above the burner rim. The volume fractions of inert
 208 gases were found to have increased relative to the distance from the fuel surface. Additionally, the
 209 maximum concentration of each species was observed at a lower z^* compared to where the
 210 maximum temperature was achieved.

211 Methanol and ethanol volume fraction profiles of H_2O and CO_2 with respect to Z^* were similar.
 212 The largest volume fractions for all product species, such as CO_2 , CO , and H_2O , were achieved
 213 when burning acetone, except for H_2 , whose peak was the lowest compared to the other fuels.
 214 Acetone was also found to produce a larger mass fraction of soot at every location along the
 215 centerline profile compared to the ethanol fire. No soot was observed in the methanol fire.

216 3.3 Comparison of Gas Species Measurements to Theoretical Values

217 Verification schemes were developed in order to assess the accuracy of the gas species
 218 measurements, carbon to hydrogen, product species, and inert species ratios were calculated and
 219 compared to theoretical values for the methanol, ethanol, and acetone pool fires. Each calculation

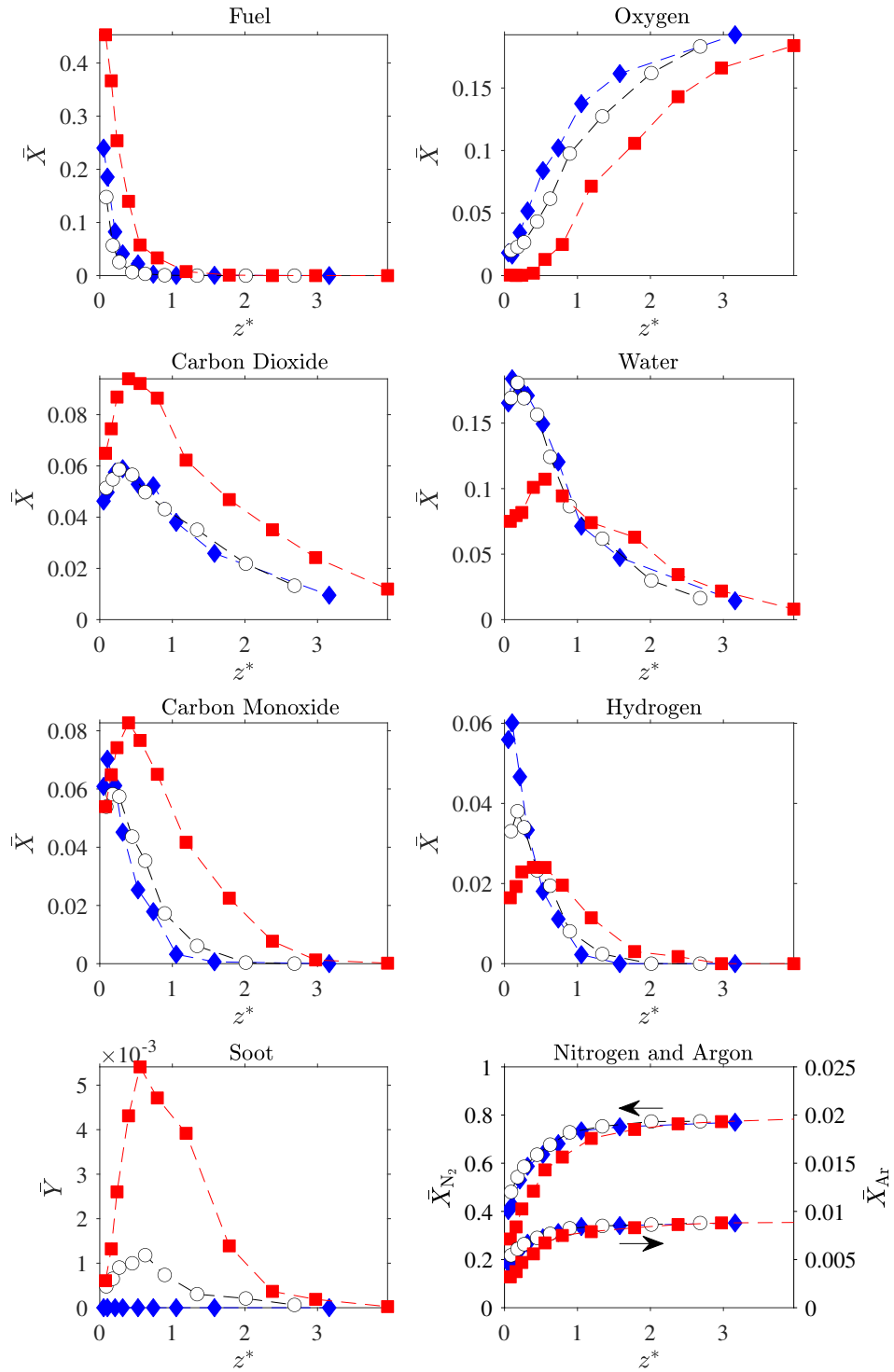


Fig. 5. Centerline volume fraction and soot mass fraction profiles of methanol (◆), ethanol (○), and acetone (■) pool fires.

220 only incorporates quantified species and assumes other identified species are trace amounts. The
 221 expanded uncertainty of the carbon to hydrogen, product, and inert ratios was determined using
 222 the law of propagation of uncertainty that accounted for the error of each volume fraction
 223 measurement.

224 The theoretical value of the carbon to hydrogen ratio was determined from the mass fraction of
 225 carbon and hydrogen residing within the parent fuel and are reported in Table 1. As shown in
 226 Eq. 9, the carbon to hydrogen ratio was calculated from the mass fraction of any quantified gas
 227 species that contained either carbon, $\bar{Y}_{i,C}$, or hydrogen, $\bar{Y}_{i,H}$. Here W_C and W_H are the molecular
 228 weights of carbon and hydrogen.

$$\frac{C}{H} = \frac{\sum \bar{Y}_{i,C} \frac{W_C}{W_i}}{\sum \bar{Y}_{i,H_2} \frac{W_{H_2}}{W_i}} \quad (9)$$

229 The carbon to hydrogen ratio for each experiment is shown in Fig. 6. The dotted line represents
 230 the theoretical value stated in Table 1. For each fuel, the data are shown to be in agreement with
 231 the theoretical value, indicating that the analysis is successful in quantifying most of the carbon
 232 and hydrogen containing species.

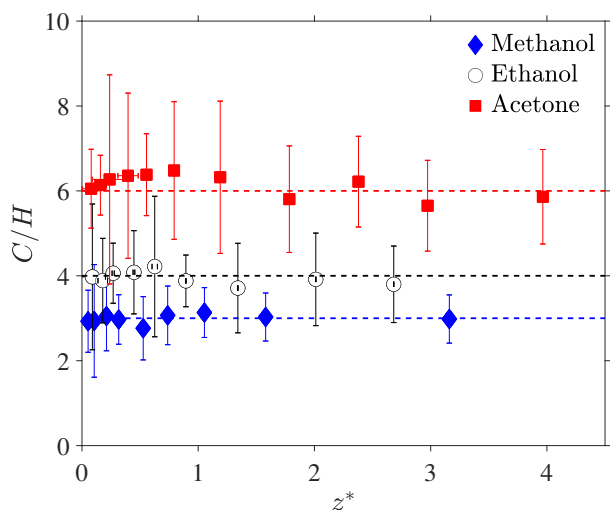
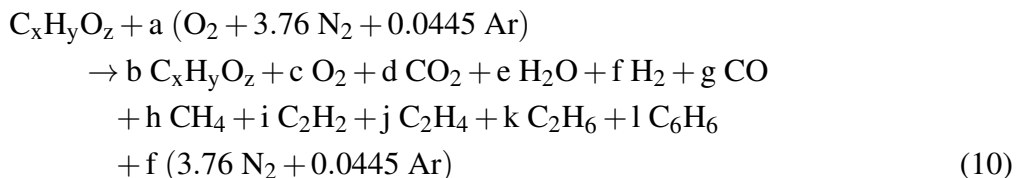


Fig. 6. Carbon to hydrogen ratio calculated from experimental values, with uncertainty bars, compared to theoretical values. Dotted lines represent the theoretical carbon to hydrogen ratio calculated from the mass fraction of carbon and hydrogen residing within the parent fuel.

Another verification test compared volume fraction measurements to stoichiometric combustion ratios, SCR, determined from the reaction below.



233 When simplified, the SCR of each fuel was calculated as:

$$\text{SCR}_{\text{methanol}} = \frac{\bar{X}_{\text{H}_2\text{O}} + \bar{X}_{\text{H}_2}}{\bar{X}_{\text{CO}_2} + \bar{X}_{\text{CO}}} = 2 \quad (11)$$

$$\text{SCR}_{\text{ethanol}} = \frac{\bar{X}_{\text{H}_2\text{O}} + \bar{X}_{\text{H}_2} + \frac{1}{2}\bar{X}_{\text{CH}_4}}{\bar{X}_{\text{CO}_2} + \bar{X}_{\text{CO}} + \frac{2}{3}\bar{X}_{\text{C}_2\text{H}_4} + 4\bar{X}_{\text{C}_6\text{H}_6}} = \frac{3}{2} \quad (12)$$

$$\text{SCR}_{\text{acetone}} = \frac{\bar{X}_{\text{H}_2\text{O}} + \bar{X}_{\text{H}_2} + \bar{X}_{\text{CH}_4} + \bar{X}_{\text{C}_2\text{H}_6}}{\bar{X}_{\text{CO}_2} + \bar{X}_{\text{CO}} + 3\bar{X}_{\text{C}_6\text{H}_6}} = 1 \quad (13)$$

234 Figure 7 shows the difference between the SCR and experimental data. The dotted lines
 235 represents the SCR values calculated from Eq. 11, 12, and 13. Direct comparison of the measured
 236 values to the idealized values shows that there is general agreement and that the volume fraction
 237 measurements are not unreasonable. An exact match is not expected since the idealized values do
 not take into account molecular diffusion, nor the mass of soot.

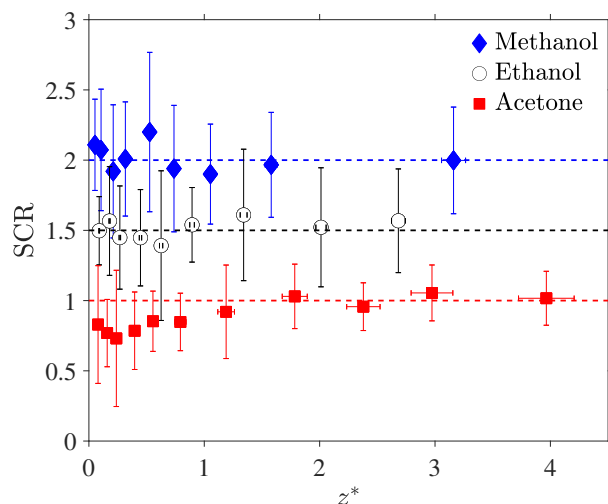


Fig. 7. Comparison of Stoichiometric Combustion Ratio, SCR, calculated from experimental and theoretical values. Dotted lines represent the theoretical SCR calculated using Eq. 12, 11, 13.

238

239 An inert ratio was also calculated from the volume fraction measurements of argon to nitrogen.
 240 Since both argon and nitrogen are inert, the ratio between them should be reasonably consistent
 241 across all fuels. The inert ratio was measured from ambient air samples using the setup described
 242 in Sec. 2.3. The inert ratio of ambient air was determined to be $0.012 \pm 4\%$. The range of the
 243 inert ratios calculated from the ambient air sample is depicted in Fig. 8 as the error band. The
 244 inert ratios determined from pool fire gas samples are shown to be within the error band region,
 245 which further supports the validity of the nitrogen and argon volume fraction measurements.

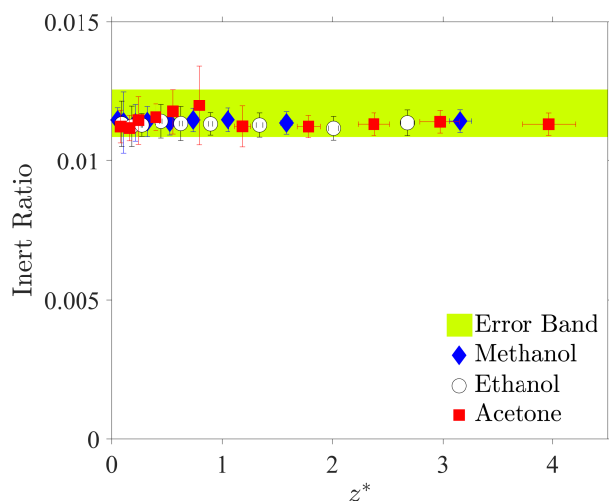


Fig. 8. Inert ratios calculated from the volume fractions for argon and nitrogen, compared to inert ratios determined from ambient air and represented as error band.

246 4. Conclusions

247 In summary, time-averaged local measurements of temperature and gas species concentrations
 248 were made to characterize the structure of methanol, ethanol, and acetone 30 cm diameter pool
 249 fire steadily burning in a quiescent environment. A verification scheme was developed to verify
 250 the gas species measurements that considered the overall stoichiometry of combustion for each
 251 fuel (see Eq. 12, 11, 13) Using this scheme, the gas species measurements were favorably
 252 compared to the idealized SCR values, which lends confidence to the veracity of the
 253 measurements. These local measurements complement previous measurements and provide
 254 insight into the complex chemical structure of medium-scale pool fires.

255 5. Acknowledgments

256 The authors would like to acknowledge Kimberly Harris of the Gas Sensing Metrology Group at
 257 NIST, who assisted in developing the species calibration method used in the study.

258 6. References

- 259 [1] K. McGrattan, S. Hostikka, R. McDermott, J. Floyd, C. Weinschenk, and K. Overholt, “Fire
 260 Dynamics Simulator, Technical Reference Guide” National Institute of Standards and
 261 Technology, Gaithersburg, Maryland, USA, and VTT Technical Research Centre of Finland,
 262 Espoo, Finland 6th edition, September 2013.
- 263 [2] S.J. Fischer, B. Hardouin-Duparc, and W.L. Grosshandler, “The structure and radiation of an
 264 ethanol pool fire,” *Combustion and Flame* vol. 70, no. 3 pp. 291–306, 1987.

- 265 [3] A. Hamins and A. Lock, "The Structure of a Moderate-Scale Methanol Pool Fire," NIST
266 Technical Note 1928 US Department of Commerce, National Institute of Standards and
267 Technology, 2016.
- 268 [4] S.C. Kim, K. Y. Lee, and A. Hamins, "Energy balance in medium-scale methanol, ethanol,
269 and acetone pool fires," *Fire Safety Journal* vol. 107, pp. 44–53, 2019.
- 270 [5] E.J. Weckman and A.B. Strong, "Experimental investigation of the turbulence structure of
271 medium-scale methanol pool fires," *Combustion and Flame* vol. 105, pp. 245–266, 1996.
- 272 [6] R. Falkenstein-Smith, K. Sung, J. Chen, and A. Hamins, "Mapping the chemical structure of
273 centerline profiles in medium-scale pool fires," NIST Technical Note, in preparation, US
274 Department of Commerce, National Institute of Standards and Technology, submitted.
- 275 [7] DIPPR[®] Constant Properties for: Methanol, Ethanol, and Acetone
276 <https://dippr.aiche.org/SampleDb>, (accessed 28 June 2019)
- 277 [8] J. Chen, Y. Zhao, X. Chen, C. Li, and C. Lu "Effect of Pressure on the Heat Transfer and
278 Flame Characteristics of Small-Scale Ethanol Pool Fires" *Fire Safety Journal* vol. 99, pp.
279 27-37, 2018.
- 280 [9] Z. Wang, W.C. Tam, K.Y. Lee, J. Chen, and A. Hamins "Thin Filament Pyrometry Field
281 Measurements in a Medium-Scale Pool Fire" *Fire Technology* accepted for publication, 2019.
- 282 [10] C.R. Shaddix, "A New Method to Compute the Radiant Correction of Bare-Wire
283 Thermocouples," 33rd ASME National Heat Transfer Conference Tenth Mediterranean
284 Combustion Symposium (MCS-10), Naples, Italy September 2017.
- 285 [11] F.P. Incropera, A.S. Lavine, T.L. Bergman, and D.P. DeWitt, *Fundamentals of heat and mass
286 transfer*, 6th Edition, Wiley, 2007.
- 287 [12] A. Hamins, S. Fischer, T. Kashiwagi, M. Klassen, and J. Gore, "Heat feedback to the fuel
288 surface in pool fires" *Combustion Science and Technology* vol. 97, no. 3, pp. 37–62, 1994.
- 289 [13] A. Hamins, M. Klassen, J. Gore, and T. Kashiwagi, "Estimate of flame radiance via a single
290 location measurement in liquid pool fires" *Combustion and Flame* vol. 86, no. 3, pp.
291 223–228, 1991.
- 292 [14] A. Lock, M. Bundy, E. Johnson, A. Hamins, G. Ko, C. Hwang, P. Fuss, and R. Harris
293 "Experimental study of the effects of fuel type, fuel distribution, and vent size on full-scale
294 underventilated compartment fires in an iso9705 room," NIST Technical Note 1603 US
295 Department of Commerce, National Institute of Standards and Technology, 2008.
- 296 [15] C.D.A. Hogben, C.N. Young, E.J. Weckman, and A.B. Strong "Radiative properties of
297 acetone pool fires," 33rd ASME National Heat Transfer Conference, Albuquerque, NM
298 August 1999.
- 299 [16] G. Heskestad "Luminous heights of turbulent diffusion flames" *Fire safety Journal* vol. 5,
300 pp.103-108, 1983.

- 301 [17] S. Pichon, G. Black, N. Chaumeix, M. Yahyaoui, J.M. Simmie, H.J. Curran, and R.
302 Donohue “The combustion chemistry of a fuel tracer: Measured flame speeds and
303 ignitiondelays and a detailed chemical kinetic model for the oxidation of acetone”
304 Combustion and Flame vol. 156, pp.494-504, 2009.
- 305 [18] J. Gong, S. Zhang, Y. Cheng, Z. Huang, C. Tang, and J. Zhang “A comparative study of
306 n-propanol, propanal, acetone, and propane combustion in laminar flames.” Proceedings of
307 the Combustion Institute vol. 35, pp.795-801, 2015.

308 **Figure captions**

309 Fig. 1. 30 cm pool burner with fuel level indicator, overflow section, and water-cooled gas
310 sampling probe.

311 Fig. 2. A schematic of the extractive sampling setup used to extract and transport fire samples
312 from the pool fire to the GC/MS.

313 Fig. 3. Snapshots of the methanol (top), ethanol (middle), and acetone (bottom) pool fires during
314 their pulsing cycles of frequency 2.6 Hz [9].

315 Fig. 4. Mean and RMS centerline temperature profiles of methanol, ethanol, and acetone pool fires
316 during their pulsing cycles with z^* expanded uncertainty.

317 Fig. 5. Centerline volume fraction and soot mass fraction profiles of methanol (◆), ethanol (○),
318 and acetone (■) pool fires.

319 Fig. 6. Carbon to hydrogen ratio calculated from experimental values, with uncertainty bars,
320 compared to theoretical values. Dotted lines represent the theoretical carbon to hydrogen ratio
321 calculated from the mass fraction of carbon and hydrogen residing within the parent fuel.

322 Fig. 7. Comparison of Stoichiometric Combustion Ratio, SCR, calculated from experimental and
323 theoretical values. Dotted lines represent the theoretical SCR calculated using Eq. 12, 11, 13.

324 Fig. 8. Inert ratios calculated from the volume fractions for argon and nitrogen, compared to inert
325 ratios determined from ambient air and represented as error band.